CrossMark

ROYAL
AERONAUTICAL
SOCIETY

REGULAR PAPER

Stabilisation, tracking and disturbance rejection control design for the UAS-S45 Bálaam

M.A.J. Kuitche, H. Yañez-Badillo, R.M. Botez* and S.M. Hashemi

ETS, Laboratory of Active Controls, Avionics and AeroServoElasticity LARCASE, 1100 Notre Dame West, Montreal, QC, Canada, H3C-1K3
*Corresponding author. Email: ruxandra.botez@etsmtl.ca

Abstract

The stabilisation and control mechanisms of an Unmanned Aerial System (UAS) must be properly designed to ensure acceptable flight performance. During their operation, these mechanisms are subjected to unknown and random environmental effects, making it imperative that all available information should be taken into consideration during the mechanisms' design process (e.g. system dynamics, actuators, flight conditions and certain criteria requirements such as phugoid and short modes for longitudinal dynamics, and roll subsidence, spiral and Dutch-roll modes for lateral dynamics) in order to guarantee flight stability. Therefore, this paper introduces a novel methodology for the stabilisation and control of the UAS-S45 Bálaam, designed and manufactured by Hydra Technologies. This methodology uses composite controllers that combine feedback Linear Quadratic Regulators (LQR) and Proportional Integral Feed-Forward (PI-FF) compensation controller for stabilisation and tracking tasks, respectively. Furthermore, a Generalised Extended State Observer was implemented to provide robustness to the closed loop dynamics by introducing disturbance compensation. Furthermore, an Adaptive Neuro-Fuzzy Inference System (ANFIS) was adopted to perform a gain scheduling by computing the gains of each composite controller for certain unknown trim conditions within a given flight domain. Finally, several numerical assessments were performed to highlight the efficiency of the proposed methodology.

Nomenclature
Symbols

A	System matrix
A$_{aug}$	Augmented system matrix
b$_d$	Disturbance vector
B	Input matrix
B$_{aug}$	Augmented input matrix
C	Output matrix
d	Disturbance
D	Feed-forward matrix
e$_p$	Steady state error
f	Uncertainty function
G	Reference gain
J	Performance index
L	Linear observer gain matrix
T$_r$	Time response at 5%
T$_{2s}$	Double amplitude time
p	Roll rate

q	Pitch rate
Q	State weighting matrix
r	Yaw rate
R	Input weighting matrix
u	Control input/x-component of the speed
v	y-component of the speed
V	speed
w	z-component of the speed
K_x	LQR gain
K_i	Proportional gain
K_p	Integral gain
K_{ff}	Feed-forward gain
K_d	GESO disturbance gain
y	System output
y_0	Controllable output
y_m	Measurable output

Greek letters

α	Angle-of-attack
ε	Error
θ	Pitch angle
ψ	Yaw angle
ϕ	Roll angle
δ_e	Elevator angle
δ_a	Aileron angle
δ_r	Rudder angle
ξ	Damping ratio
ω	Natural frequency
τ	Time constant

Abbreviation

ANFIS	Adaptive Neuro-Fuzzy Inference System
GESO	Generalised Extended State Observer
LQR	Linear Quadratic Regulator
LPV	Linear Parameter Varying
PI-FF	Proportional Integral with feed-forward compensation
PSO	Particles Swarm Optimisation
UAS	Unmanned Aerial System

1.0 Introduction

Achieving accurate control for Unmanned Aerial Systems (UAS) is complicated. The diversity of mission platforms, nonlinear dynamics, resource constraints and unpredictable environmental conditions are some of the main problems. An efficient solution to these problems requires the utilisation of flight control systems that are highly resilient and autonomous, capable of guaranteeing constraints satisfaction, robustness and reliability in the range of model flight dynamics and operating conditions [1, 2]. The recent interests in making Unmanned Aerial Systems [3]–[5] more robust, and in increasing their abilities have led researchers to address these challenging demands using modern controller synthesis approaches.

Optimal control [6]–[9] is a commonly applied method that seeks to maximise the desired system outputs for a minimum cost. Zhen et al. [10] investigated anti-wind attitude control for the Boeing 707 in the landing phase. The longitudinal attitude control was based on the Proportional Integral Derivative (PID) and the C* inner control, whereas the lateral attitude control was performed using an optimal regulator.

In [11], a Linear Quadratic Regulator (LQR) control strategy was applied on a two-degree-of-freedom laboratory helicopter for pitch and yaw angle controls. Their methodology used the adaptive Particle Swarm Optimisation (PSO) algorithm to improve the selection of control gains, and to guarantee an optimal attitude tracking control. Even if optimal control is considered as the universal solution for linear control problems [12], bibliographical research publications [13–15] pointed out that its robustness is not guaranteed.

In addition to the optimal control, robust control methods [16, 17] may be applied when the aircraft dynamic uncertainties are considered. Boughari et al. [18] proposed a robust controller that was optimised on an optimisation using the H_∞ method, and the genetic algorithm for the Cessna Citation X. This controller was designed to ensure acceptable flying qualities in the presence of aircraft dynamics uncertainties dues to mass and centre of gravity variations. Liu et al. [19] proposed a Model Predictive Control (MPC) based on a Linear Quadratic Gaussian (LQG) approach to compensate for the dynamic gust loads on the flexible aircraft in turbulence conditions. This association of the MPC and the LQG methods makes it possible to manage the problems of dynamics variation and disturbance rejection, and thereby to ensure a robust performance. Pavel et al. [20, 21] implemented a nonlinear control scheme using the Incremental Nonlinear Dynamic Inversion (INDI) methodology on an Apache AH-64D Longbow helicopter model. Their goal was to provide improved handling qualities for hover and low-speed flights. Simplicio et al. [22] developed an acceleration measurement-based control using the INDI technique to cope the need of aerodynamics data. Both methodologies showed an increased robustness to model uncertainties. Some cases of robust control lead to high-order controllers which are difficult to implement in practical situations without reducing their order [23]. However, a reduction of a controller also affects its performance.

Another option is to use intelligent control [24–26]. In [27], a longitudinal dynamics controller based on a Takagi-Sugeno fuzzy model was presented. The controller was applied to the twin-engine short-range transport aircraft LET L410 to guarantee closed loop stability and pitch angle tracking. Duong et al. [28, 29] designed a hybrid controller based on a PI and a fuzzy control for wind turbine applications. The fuzzy control methodology improved the PI controller by smoothing the influence of parameter variation, which led further to an effective pitch angle control. Another methodology proposed by Grimaccia et al. [30] used a neuro-fuzzy method to improve the energy production of photovoltaic plants. The proposed neuro-fuzzy algorithm helped to solve complex interaction and nonlinearities among input data (weather) to forecast energy production. Wu et al. [31] developed an adaptive neural network flight control for aircraft longitudinal motion in high angle-of-attack conditions. Their adaptive neural network was designed using a coupling of a variable separation technique with the Lyapunov–Krasovski function method. The methodology showed good performance for an uncertain non-strict feedback nonlinear system with distributed time-varying delays. However, classical neural network architecture requires a large amount of training data in order to perform an accurate interpolation. Furthermore, the neural network weights do not represent physical variables, thus neural network architectures are difficult to adjust in practical situations.

In addition, increasingly development and implementation of several disturbance estimation mechanisms has been shown in the literature, such as the Disturbance Observer (DO), Unknown Input Observer (UIO), Perturbation Observer (PO) and Extended State Observer (ESO) [32]. The ESO mechanism has been chosen for handling disturbance estimation in efficient active disturbance rejection control theory [33], which allows to estimate and compensate the unmodelled dynamics, parametric uncertainty, and external disturbances. Nevertheless, the standard approach is designed for integral chain systems where the matching condition is satisfied. Thus, for solving the disturbance rejection problem in flight control systems, the Generalised Extended State Observer (GESO) based controller has been successfully implemented in aerial systems [34]. Another interesting approach for solving the trajectory tracking and path following for different kinds of vehicles subjected to disturbances may be composed by improved disturbance estimators. In [35], a Nonlinear Disturbance Observer (NDO) was used to provide robustness to the closed loop control scheme, in which a Back-Stepping-base control was performed for the stabilisation and tracking tasks of a quadrotor UAV. In the same way, the simulation results presented in

[36] have shown that observers were successfully implemented with the aim to improve the robustness of a marine surface vessel, that was also subjected to environment disturbances: wave drift, currents and mean wind forces.

To capture the benefits of each of these control methodologies, a design approach is introduced in this paper. The aim of the approach is to provide a robust low-order controller able to solve a nonlinear control problem. In the case of aircraft control, the states of the aircraft vary over time due to the environment (altitude, wind, etc.) or its configuration (cg position, weight, etc.) which transform the linear problem into a nonlinear problem.

The overall controller architecture is composed by a Linear Quadratic Regulator (LQR) feedback controller to ensure aircraft stability, and a Proportional-Integral controller combined with reference Feed Forward compensation (PI-FF) to provide an accurate controllability in case of error in data. This controller can be easily implemented in practical situations because of its low order. In addition, a Generalised Extended State Observer (GESO) was added to the controller design for robustness improvement. The GESO is a very good alternative to design a robust controller since it allows the estimation and compensation of disturbances and uncertainties [37, 38]. Finally, a Linear Parameter-Varying (LPV) method was applied to provide a nonlinear capability to the controller. The proposed scheme uses a minimum amount of data to handle the nonlinear problem. The LPV method is based on an Adaptive Neuro-Fuzzy Inference System (ANFIS) which is a combination of a fuzzy theory and a neural network. The fuzzy theory provides additional data to the neural network in order to enhance its ability to produce the estimated outputs. This approach reduces the number of operating points required by use of the fuzzy logic technique to complete the unknown data.

The main contribution of this paper lies in the methodology proposed to design each part of the controller. The efficiency of the methodology is proved by the controller reliability in the presence of various disturbances. The robustness of the controller was ensured using two methodologies: The first methodology was the eigenvalues (pole and zeros) placement. This methodology was performed using a stability domain defined by the Hurwitz stability theory. The optimal controller and PID gains were selected, so that the poles and zeros lied in this domain, and thus they ensured a stable dynamic with a level 1 qualification (can handle perturbations around a trimmed position) according to the MIL-STD-1797A standard [39, 40]. An automatic process using the Particle Swarm Optimisation (PSO) was then used to ensure that all the selected gains covered this domain. The second methodology was the implementation of a Generalised Extended State Observer (GESO) to ensure additional robustness, as it can estimate and compensate the unmodelled dynamics, parametric uncertainty, and external disturbances. In the literature, the GESO based control have been successfully implemented in several dynamic systems such as marine vessels, quadrotor aerial vehicles, magnetic levitation suspensions, missile longitudinal autopilots, charge of a super capacitors, wheeled mobile robots, among others [41–44]. In the present manuscript the effectiveness of GESO design for robustness of the UAS-S45 Bálaam system output is demonstrated.

The paper is organised as follows. The UAS-S45 model and its dynamic equations are presented in Section 2 (the actuator dynamics and the hinge moment of the control surfaces are considered in the introduced model), followed by the control scheme in Section 3. It consists of a LQR for stability augmentation, a PI-FF for the control augmentation, and a GESO for improving robustness capabilities. The LPV based on the ANFIS method is described in Section 4. Finally, Section 5 presents and discusses the simulation results, and is followed by Conclusions.

2.0 UAS-S45 Bàlaam dynamic equations

The proposed control methodology was applied to the flight dynamics model of the UAS-S45 Bálaam. The UAS-S45 is an Unmanned Aerial System designed and manufactured by Hydra Technologies to provide surveillance and security capabilities for both military and civilian purposes [45](Fig. 1). Its general characteristics are given in Table 1.

Table 1. *General characteristics of the UAS-S45*

Specification	Value
Wing span	6.11 m
Wing area	2.72 m^2
Total length	3.01 m
Mean aerodynamic chord	0.57 m
Empty weight	57 kg
Maximum take-off weight	79.6 kg
Loitering airspeed	55 knots
Service ceiling	20, 000 ft
Operational range	120 km

Figure 1. *The UAS-S45 Bálaam.*
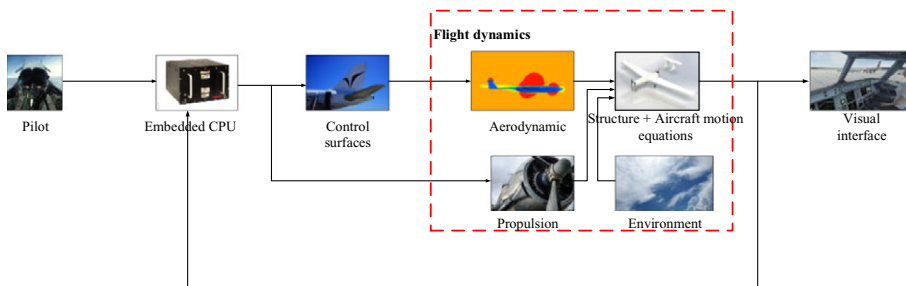
Figure 2. *The UAS-S45 simulation model.*

Kuitche and Botez [46] have developed a flight dynamics model of the UAS-S45 (Fig. 2). Their flight dynamics model was designed to evaluate the performance of a morphing wing technique. Its architecture was divided in four sub-models and each of these sub-models was estimated using numerical and experimental methodologies.

The authors described the flight dynamics model and presented the results of its accuracy. For convenience purpose, this paper is cited in the text for readers to present the design and accuracy of the model.

The aerodynamic sub-model was realised by a combination of the contributions of the 'wing part', the 'fuselage part', the 'tail part', and their interactions. Its estimation was performed using Fderivatives code [47–49], which is an improvement of the DATCOM procedure using new CFD analyses methodologies.

The propulsion sub-model is a piston-propeller engine model. The piston engine was designed using equations derived from the ideal Otto cycle and was optimised using the manufacturer's data. The propeller aerodynamic performance was obtained using a CFD analysis and the Blade Element Theory (BET).

The structural sub-model determines the mass and inertia of the UAS-S45 using the Raymer equations [46] and the DATCOM procedure.

The actuator sub-model was estimated using a servomotor model and mechanical calculations.

Each sub-model was validated using experimental or real data. The results showed a very good agreement between estimated and experimental or real data.

The UAS-S45 flight dynamics model developed by Kuitche and Botez [46] was obtained for several regimes, including cruise, take-off and landing, and for various flight conditions. This model is therefore used for controller design.

The state-space representations for the longitudinal and the lateral dynamics of the UAS-S45 model are given by Equation (1) and Equation (2), respectively:

$$
\begin{bmatrix} \Delta\dot{u} \\ \Delta\dot{w} \\ \Delta\dot{q} \\ \Delta\dot{\theta} \end{bmatrix} = \begin{bmatrix} X_u & X_w & 0 & -g \\ Z_u & Z_w & u_0 & 0 \\ M_u + M_{\dot{w}}Z_u & M_w + M_{\dot{w}}Z_w & M_q + M_{\dot{w}}u_0 & 0 \\ 0 & 0 & 1 & 0 \end{bmatrix} \begin{bmatrix} \Delta u \\ \Delta w \\ \Delta q \\ \Delta\theta \end{bmatrix}
$$

$$
+ \begin{bmatrix} X_{\delta_e} & X_{\delta_T} \\ Z_{\delta_e} & Z_{\delta_T} \\ M_{\delta_e} + M_{\dot{w}}Z_{\delta_e} & M_{\delta_T} + M_{\dot{w}}Z_{\delta_T} \\ 0 & 0 \end{bmatrix} \begin{bmatrix} \Delta\delta_e \\ \Delta\delta_T \end{bmatrix} \tag{1}
$$

$$
\begin{bmatrix} \Delta\dot{v} \\ \Delta\dot{p} \\ \Delta\dot{r} \\ \Delta\dot{\phi} \end{bmatrix} = \begin{bmatrix} Y_v & Y_p & -(u_0 - Y_r) & g\cos(\theta_0) \\ L_v & L_p & L_r & 0 \\ N_v & N_p & N_r & 0 \\ 0 & 1 & 0 & 0 \end{bmatrix} \begin{bmatrix} \Delta v \\ \Delta p \\ \Delta r \\ \Delta\phi \end{bmatrix} + \begin{bmatrix} 0 & Y_{\delta_r} \\ L_{\delta_a} & L_{\delta_r} \\ N_{\delta_a} & N_{\delta_r} \\ 0 & 0 \end{bmatrix} \begin{bmatrix} \Delta\delta_a \\ \Delta\delta_r \end{bmatrix} \tag{2}
$$

where u, v, and w are the velocity components around the body axes, p, q and r are the angular velocity components, θ and ϕ are respectively the pitch and the roll angle, δ_e is the elevator angle, δ_a is the aileron angle, δ_r is the rudder angle, and δ_T is the throttle position. X_u, X_w, X_δ, Y_v, Y_p, Y_r, Y_δ, Z_u, Z_w, Z_δ, L_v, L_p, L_r, L_δ, M_u, M_w, M_δ, and N_v, N_p, N_r, N_δ are the stability derivatives. The uncoupled dynamics was considered because the robust controller could handle the unmodelled flight dynamics around an equilibrium position.

3.0 Introduction of control schemes in the UAS-S45 flight dynamics model

3.1 The proposed controller

Figure 3 shows the control system for the UAS-S45 flight dynamics model. The controller is composed of a Stability Augmentation System, a Proportional Integral Feed Forward controller for controllability augmentation and a Generalised Extended State Observer for robustness improvement.

The associated control law is given by:

$$
\Delta u = -K_x\Delta\hat{x} - K_i\Delta\varepsilon + K_p\Delta\dot{\varepsilon} + K_{ff}r + K_d\hat{d} \tag{3}
$$

where K_x is the SAS (Stability Augmentation System) vector gain, K_i is the integral gain, K_p is the proportional gain, K_{ff} is the feed-forward gain, K_d is the GESO disturbance gain, u is the control input, $\hat{x}$ is the estimated state vector and $\Delta\dot{\varepsilon}$ is the error between the input reference, the measured output,

Table 2. *Stability augmentation system criteria*

Dynamic mode	Specifications
Phugoid	$\xi_{ph} \geq 0.04$
Short period	$0.35 \leq \xi_{sp} \leq 1.30$
Dutch roll	$\xi_{dr} \geq 0.19$
	$\omega_{dr} \geq 1.0\,\text{rad/s}$
	$\xi_{dr}\,\omega_{dr} \geq 0.35\,\text{rad/s}$
Spiral	$T_{2s} \geq 12\,\text{s}$
Roll subsidence	$\tau_{ra} \leq 1.0\text{s}$

Table 3. *Tracking step criteria*

Criteria	Specifications
Maximum overshoot (D)	$D \leq 5\%$
Time response at 5% (T_r)	$T_r \leq 6\text{s}$
Steady state error (e_p)	$e_p \leq 10^{-2}$
Margin gain	$MG \leq 6\,\text{dB}$
Margin Phase	$MP \geq 45°$
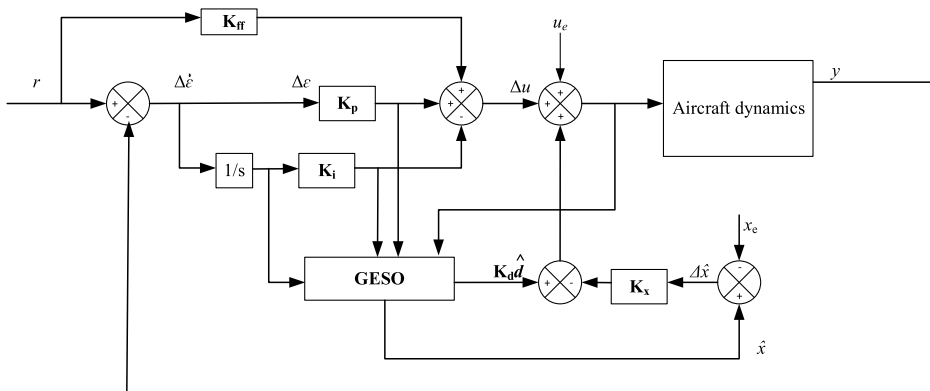
Figure 3. *The UAS-S45 Control Law.*

u_e is the control input at the equilibrium position and x_e is the state vector at the equilibrium position. Figure 3 shows the general description of the controller that was used for the pitch and roll channels. For the pitch channel, the control input used was the elevator deflection, whereas for the roll channel, the control inputs used were given by the aileron and rudder deflections.

Since the UAS-S45 is useful for military purposes, such as intelligence gathering and surveillance, it requires specific flight qualities to guarantee a proper flight performance. The flight quality requirements provided by the *"U.S. Military Specification for the Flying Qualities of Piloted Airplanes MIL-STD-1797A"* [50, 51] defined in terms of damping and natural frequency were therefore used for this analysis. These requirements were chosen by assuming that the UAS-45 is a light aircraft and are listed in Table 2 for each dynamic mode response (short period, phugoid, roll subsidence, spiral and Dutch roll), and in Table 3 for a tracking step response or criteria.

In Table 2, ξ and ω are the damping and the frequency, respectively, of the considered mode, τ_{ra} is the time constant, and T_{2s} is the double amplitude time given by:

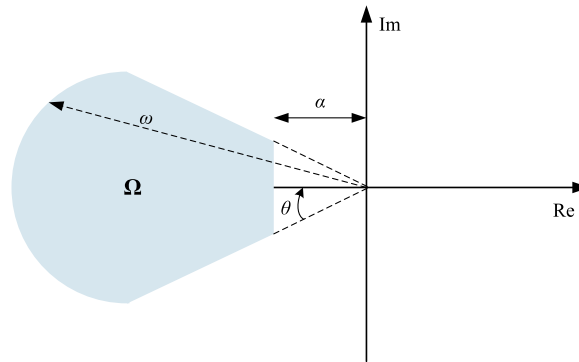$$T_{2s} = \frac{-\ln(2)}{\xi\omega} \tag{4}$$

Figure 4. *The stability domain representation.*

3.2 Design methodology of the controller

The main contribution of this paper lies in the methodology proposed to obtain the controller gains shown in Equation (3). For this purpose, the state-space representation of the UAS-S45 dynamics is described by Equations (1) and (2), which are given in the form of a Linear Time Invariant (LTI) system [52–54]. Equation (5) shows the state space representation of the system used for the controller design. This equation is referred to in the design steps of the controller.

$$\Delta\dot{\mathbf{x}} = \mathbf{A}\Delta\mathbf{x} + \mathbf{B}\Delta\mathbf{u}$$
$$\Delta\mathbf{y} = \mathbf{C}\Delta\mathbf{x} + \mathbf{D}\Delta\mathbf{u}$$
(5)

where **A**, **B**, **C** and **D** are the system, the input, the output and the feed-forward matrices, respectively, *x* is the state vector, *u* is the control vector, and *y* is the output vector.

Definition 1: Let Ω be an open subset of the complex plane, **A** is a n × n real matrix and $\Lambda(\mathbf{A})$ are the eigenvalues of **A**.

A is said to be stable relative to Ω if $\Lambda(\mathbf{A}) \subseteq \Omega$.

Thus, the generalised stability set which represents the set of all matrices stable relative to Ω is given by:

$$S(\Omega) = \left\{ A \in \mathbb{R}^{n \times n} \colon \Lambda(\mathbf{A}) \subset \Omega \right\}$$
(6)

Due to the need of the LTI system to respect the flight requirements given in Tables 2 and 3, the general stability problem (Hurwitz stability) is transformed into a relative stability problem. Figure 4 shows a representation of the stability domain where $\theta = \cos^{-1}\xi$ is the angle defined using the damping ξ, ω is the natural frequency and α is the half plane shift.

The proposed methods to obtain the gains K_x, K_i, K_p, K_{ff} and K_d are performed in the next three steps:

Step 1: Design of a Linear Quadratic Regulator (LQR) using a selection technique for the weight matrices. The LQR method was used to ensure the dynamic mode (short period, phugoid, roll subsidence, spiral, Dutch roll) stability of the UAS-S45. An additional state was added to the LTI system described in Equation (5) for considering pitch angle steady-state error, therefore the following expression is obtained:

$$\begin{bmatrix} \Delta\dot{x} \\ \Delta\dot{\varepsilon} \end{bmatrix} = \mathbf{A}_{\text{aug}} \begin{bmatrix} \Delta x \\ \Delta\varepsilon \end{bmatrix} + \mathbf{B}_{\text{aug}} \Delta u + \begin{bmatrix} \mathbf{0}_{i\times 1} \\ 1 \end{bmatrix} r, \text{ where } \mathbf{A}_{\text{aug}} = \begin{bmatrix} \mathbf{A} & \mathbf{0}_{i\times 1} \\ -\mathbf{C} & 0 \end{bmatrix}, \text{ and } \mathbf{B}_{\text{aug}} = \begin{bmatrix} \mathbf{B} \\ \mathbf{0}_{1\times j} \end{bmatrix}$$
(7)

In Equation (7) $\mathbf{A}_{\text{aug}}$ and $\mathbf{B}_{\text{aug}}$ are the augmented matrices, *i* is the row number of **A**, and *j* is the column number of **B**.

The LQR approach needed to obtain an optimal solution of a control problem is given in [55–57]. The LQR method is applicable if the system is controllable. The LQR methodology is based on the minimisation of the next cost function:

$$J = \frac{1}{2} \int_0^\infty \left(x^T \mathbf{Q} x + u^T \mathbf{R} u \right) dt \tag{8}$$

where x is the state, u is the control input, and $\mathbf{Q}$ and $\mathbf{R}$ are the positive weighting matrices.

The optimal gain $\mathbf{K}$ is obtained using the following expression:

$$\mathbf{K} = \mathbf{R}^{-1} \mathbf{B}^{\mathbf{T}} \mathbf{P} = \begin{bmatrix} \mathbf{K}_x & \mathbf{K}_{ss} \end{bmatrix} \tag{9}$$

where $\mathbf{P}$ is the Riccati's matrix, $\mathbf{B}$ is state space input matrix. $\mathbf{K}_x$ is the feedback control gain vector, and $\mathbf{K}_{ss}$ is an integral gain which was replaced by the control augmentation system.

In [11, 53, 55, 57], the weighting matrices $\mathbf{Q}$ and $\mathbf{R}$ of the LQR methodology are manually selected; therefore, it is not guaranteed that the system to be controlled will meet some specific requirements. To ensure that the stabilised UAS-S45 will meet the desired flight qualities, the Q and R weighting matrices are selected in this paper using an optimisation procedure based on the metaheuristic Particle Swarm Optimisation (PSO) algorithm.

The PSO was bounded for the weighting matrices' selection to reduce the search space, and to ensure that the matrices would be positively defined at each iteration. An objective function was proposed in Equation (10) to evaluate the convergence of the optimisation algorithms:

$$J_1 = \min_{\mathbf{K}} \left[(N - n_c) \times 10^5 + \sum_j \left(\mathbf{K}_j \right)^2 \right] \tag{10}$$

where n_c is the number of requirements that are met in each iteration, N is the total number of criteria, and $\mathbf{K}_j$ represent the jth element in the vector $\mathbf{K}$. The expression $\sum_j \left(\mathbf{K}_j \right)^2$ is added to the objective function to reduce the size of control vector gains parameters.

The overall process that takes place to illustrate the LQR methodology and obtain the LQR control vector gain is summarised in Fig. 5.

Step 2: The Proportional-Integral with reference Feed-Forward (PI-FF) gains were evaluated for the stabilised system. A PI-FF controller was used to address the tracking problems. It is mainly composed of a Proportional Integral (PI) controller. Due to its stable, reliable and easy-to-adjust structure, the PI controller remains one of the main controller for industrial purposes [58]. The PI controller is suitable for stabilising a system and for eliminating the steady state error. Moreover, in order to improve the tracking performance, a reference feed-forward compensator was added to the PI controller [59]. The reference feed-forward compensator can anticipate the reference modification before the PI controller and can provide an additional command.

The state space representation of the closed loop system used in this step is given by:

$$\begin{bmatrix} \Delta \dot{x} \\ \Delta \dot{\varepsilon} \end{bmatrix} = \begin{bmatrix} \mathbf{A} + \left(\mathbf{K}_x - \mathbf{K}_p \right) \mathbf{BC} & \mathbf{K}_i \mathbf{B} \\ -\mathbf{C} & 0 \end{bmatrix} \begin{bmatrix} \Delta x \\ \Delta \varepsilon \end{bmatrix} + \begin{bmatrix} \left(\mathbf{K}_p + \mathbf{K}_{ff} \right) \mathbf{B} \\ 1 \end{bmatrix} [r] \tag{11}$$

$$y = \begin{bmatrix} \mathbf{C} & 0 \end{bmatrix} \begin{bmatrix} \Delta x \\ \Delta \varepsilon \end{bmatrix}$$

Which can be referred for simplicity to:

$$\begin{bmatrix} \Delta \dot{x} \\ \Delta \dot{\varepsilon} \end{bmatrix} = \mathbf{A}_{cl} \begin{bmatrix} \Delta x \\ \Delta \varepsilon \end{bmatrix} + \mathbf{B}_{cl} [r] \tag{12}$$

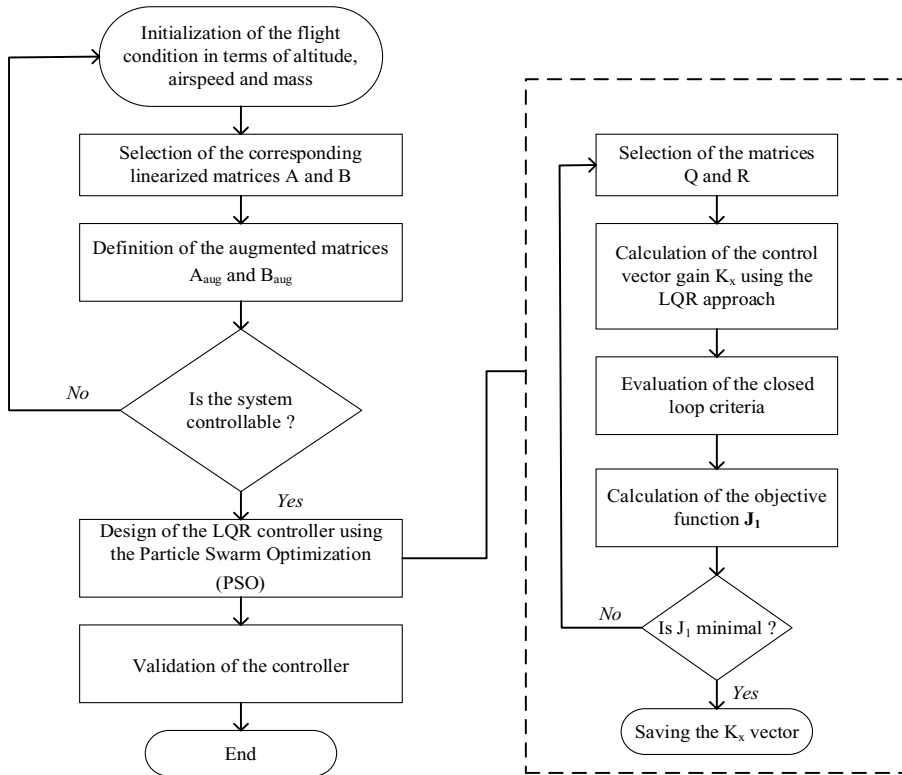$$y = \mathbf{C}_{cl} \begin{bmatrix} \Delta x \\ \Delta \varepsilon \end{bmatrix}$$

Figure 5. *LQR Control Process.*

The gains were estimated using the same objective function J_1 and the PSO algorithm. The overall process to obtain the $\mathbf{K_i}$, $\mathbf{K_p}$ and $\mathbf{K_{ff}}$ parameters is summarised in Fig. 6.

It is important to note that the evaluation of the closed loop criteria also considers the verification of the closed loop stability of the overall system.

Step 3: Although the relative stability of the overall system is verified while the control gains selection in steps 1 and 2, its robustness is not guaranteed (the selected gains could be located at the boundary of the stability domain). As the final goal is to perform a gain scheduling, it is essential to ensure that the controller can resist to disturbances, and to model variation. Therefore, the Generalised Extended State Observer (GESO) was added to the control system. For the purposes of GESO design, an alternative representation of the augmented model introduced in Equation (5) is considered:

$$\Delta\dot{\mathbf{x}}_{\mathrm{aug}} = \mathbf{A}_{\mathrm{aug}}\Delta\mathbf{x}_{\mathrm{aug}} + \mathbf{B}_{\mathrm{aug}}\Delta\mathbf{u} + \mathbf{G}r \tag{13}$$

Unmodelled dynamics, parametric uncertainties and external disturbances can then be introduced in the analysis by adding them into the UAS-S45 system model given in Equation (13) as follows:

$$\begin{aligned}
\Delta\dot{x}_{\mathrm{aug}} &= \mathbf{A}_{\mathrm{aug}}\Delta x_{\mathrm{aug}} + \mathbf{B}_{\mathrm{aug}}\Delta u + \mathbf{G}r + \mathbf{b}_d d \\
y_m &= \mathbf{C}_m\Delta\mathbf{x}_{\mathrm{aug}} \\
y_o &= \mathbf{C}_o\Delta\mathbf{x}_{\mathrm{aug}}
\end{aligned} \tag{14}$$

where d are the disturbances or uncertainties, $\boldsymbol{b}_d$ is a disturbance matrix, y_m is the measurable output, y_o is the controllable output, $\mathbf{C}_o = [\mathbf{C}\ 1]$ and $\mathbf{C}_m = \begin{bmatrix} 0 & 0 & 0 & 1 & 0 \\ 0 & 0 & 0 & 0 & 1 \end{bmatrix}$. For design purposes, m represents the row number of $\mathbf{A_{aug}}$, and n is the column number of $\mathbf{B_{aug}}$.
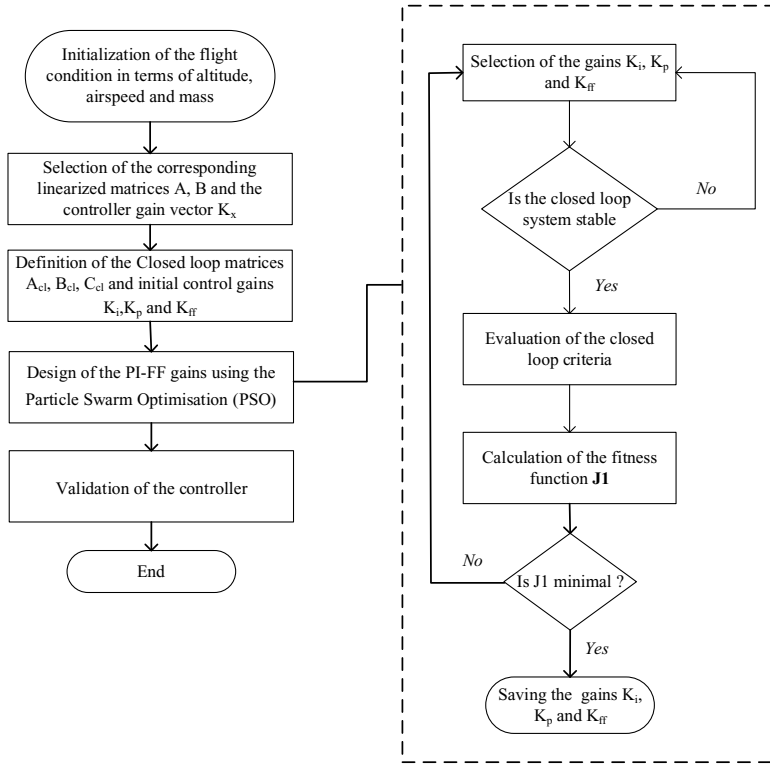
Figure 6. *PI-FF gains estimation process.*

Then, by considering the methodology described in [60], the extended state-space system can be expressed as:

$$\dot{\bar{x}} = \bar{\mathbf{A}}\bar{x} + \bar{\mathbf{b}}_u \Delta u + \bar{\mathbf{G}}r + \mathbf{E}h$$
$$y_m = \bar{\mathbf{C}}_m \bar{x} \tag{15}$$

where

$$\bar{\mathbf{A}} = \begin{bmatrix} \mathbf{A}_{\text{aug}} & \mathbf{b}_d \\ \mathbf{0}_{1 \times m} & 0 \end{bmatrix}, \bar{x} = \begin{bmatrix} \Delta x_{\text{aug}} \\ \Delta x_{m+1} \end{bmatrix}, \text{with} \Delta x_{m+1} = d \tag{16}$$

$$\mathbf{E} = \begin{bmatrix} \mathbf{0}_{m \times 1} \\ 1 \end{bmatrix}, \bar{\mathbf{b}}_u = \begin{bmatrix} \mathbf{B}_{\text{aug}} \\ \mathbf{0}_{1 \times n} \end{bmatrix} \tag{17}$$

and

$$\bar{\mathbf{G}} = \begin{bmatrix} \mathbf{G} \\ 0 \end{bmatrix}, \bar{\mathbf{C}}_m = [\mathbf{C}_m \ \mathbf{0}_{2 \times 1}] \tag{18}$$

If the pair $(\mathbf{A}_{\text{aug}}, \mathbf{B}_{\text{aug}})$ is controllable, and $(\bar{\mathbf{A}}, \bar{\mathbf{C}}_m)$ is observable, the GESO of the system described in Equation (13) can be expressed as:

$$\dot{\hat{\bar{x}}} = \bar{\mathbf{A}}\hat{\bar{x}} + \bar{\mathbf{b}}_u \Delta u + \bar{\mathbf{G}}r - \mathbf{L}(y_m - y_m)$$
$$y_m = \bar{\mathbf{C}}_m \hat{\bar{x}} \tag{19}$$

Table 4. *Flight conditions for the gain scheduling method*

Altitude [m]	Airspeed [m/s]	Mass [kg]
0–6000	26–45	53–76

where $\mathbf{L}$ is the linear observer gain matrix, and $\hat{\bar{x}}$ is the estimated value of $\bar{x}$. The same feedback controller introduced in Equation (10) is used. For the disturbance rejection tasks, as stated in [34], if the next condition is satisfied:

$$\mathbf{C}_o\left(\mathbf{A}_{\text{aug}} - \mathbf{B}_{\text{aug}}\mathbf{K}_x\right)^{-1}\mathbf{B}_{\text{aug}}K_d = -\mathbf{C}_o\left(\mathbf{A}_{\text{aug}} - \mathbf{B}_{\text{aug}}\mathbf{K}_x\right)^{-1}\mathbf{b}_d \quad (20)$$

the disturbance gain can be solved from the above expression if the following rank condition is true

$$\begin{aligned}
&\text{rank}\left(\mathbf{C}_o\left(\mathbf{A}_{\text{aug}} - \mathbf{B}_{\text{aug}}\mathbf{K}_x\right)^{-1}\mathbf{B}_{\text{aug}}\right) = \\
&\text{rank}\left(\left[\mathbf{C}_o\left(\mathbf{A}_{\text{aug}} - \mathbf{B}_{\text{aug}}\mathbf{K}_x\right)^{-1}\mathbf{B}_{\text{aug}}, -\mathbf{C}_o\left(\mathbf{A}_{\text{aug}} - \mathbf{B}_{\text{aug}}\mathbf{K}_x\right)^{-1}\mathbf{b}_d\right]\right)
\end{aligned} \quad (21)$$

Then, the designed disturbance gain is given as follows,

$$K_d = -\left[\mathbf{C}_o\left(\mathbf{A}_{\text{aug}} - \mathbf{B}_{\text{aug}}\mathbf{K}_x\right)^{-1}\mathbf{B}_{\text{aug}}\right]^{-1}\mathbf{C}_o\left(\mathbf{A}_{\text{aug}} - \mathbf{B}_{\text{aug}}\mathbf{K}_x\right)^{-1}\mathbf{b}_d \quad (22)$$

where $\mathbf{K}_x$ is the gain vector obtained in Equation (9). The GESO robust scheme was implemented for both longitudinal and lateral dynamics modeling.

Notice that the controller design methodology described in Section 3 is applied for a linear state space representation locally defined around an operating point which may be subjected to disturbances. However, aircraft dynamics can change drastically from one operating flight point to another. Thus, there is a need for nonlinear control laws design that can consider the flight dynamics' variations with the flight conditions.

4.0 Extension of the method for solving the nonlinear control problem using an adaptive neuro-fuzzy inference system (ANFIS)

Gain scheduling is an effective method to design nonlinear flight control laws using a linear control technique [61]. A specific type of gain scheduling called the Linear Parameter-Varying (LPV) system is utilised in this work. Depending on the variation of the exogenous parameters (generally for their strong variations), the gain-scheduled controller can lose its effectiveness (loss of stability and robustness).

The LPV system is thus restricted to the "slow variation" of parameters [61]. Conventionally, the "slow variation" problem is addressed by increasing the number of operating points required for the gain scheduling, which has the consequence of increasing the computational time and the amount of resources needed. The proposed LPV system is based on the Adaptive Neuro-Fuzzy Inference System (ANFIS) [62]. This approach reduces the number of operating points required by use of the fuzzy logic technique to complete the unknown information. The Neural Network component in the ANFIS [63–65] thus increases the interpolation capacity of its fuzzy logic technique.

The procedure to obtain a gain-scheduled controller using the ANFIS is composed of four steps:

Step 1: The flight envelope domain takes into consideration several flight conditions. A number of 216 flight conditions were considered in terms of altitude, airspeed and aircraft mass. For each flight condition, a linearisation process was performed for the longitudinal and lateral dynamics modeling. Figure 7 shows the flight domain, as well as the flight conditions, which are listed in Table 4.

Step 2: For each flight condition, a local linear controller, as the one established in Equation (3), was designed following the flight qualities' requirements described in Section 3. The gains parameters K_x, K_i, K_p, K_{ff} and K_d were determined, and further mapped as functions of the altitude, airspeed and mass.

Step 3: The scheduling was performed to evaluate the parameters of the controller for an unknown trim condition. The ANFIS was used for this purpose. The general ANFIS architecture, presented in Fig. 8,
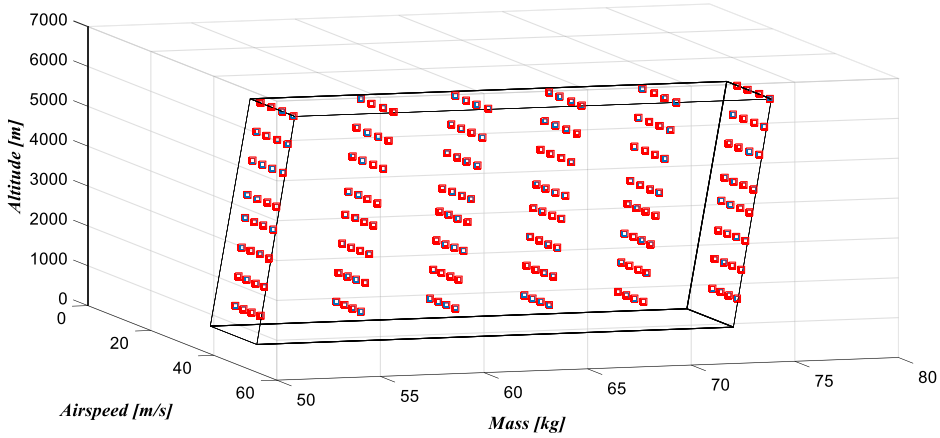
Figure 7. *Flight domain with the flight conditions for the gain scheduling.*
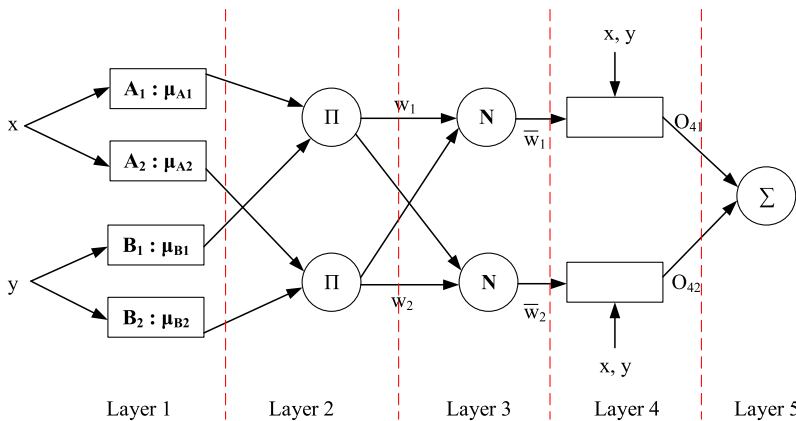

Figure 8. *General ANFIS architecture [66].*

is based on the Takagi-Sugeno fuzzy inference system [66], defined as:

$$
\begin{aligned}
\text{Rule1} &= \text{If } x \text{ is } A_1 \text{ and y is } B_1, \quad \text{Then } f_1 = p_1 x + q_1 y + r_1 \\
\text{Rule2} &= \text{If } x \text{ is } A_2 \text{ and y is } B_2, \quad \text{Then } f_2 = p_2 x + q_2 y + r_2
\end{aligned}
\tag{23}
$$

The ANFIS architecture has five layers, as shown in Fig. 8. In layer 1, the output of each node is the membership function μ_{Ai} and specifies the degree to which the given input is similar to A_i. The proposed gain scheduling methodology used four generalised bell-shaped membership functions defined as follows:

$$
\mu_{A_i}(x) = \frac{1}{1 + \left| \frac{x - c_i}{a_i} \right|^{2b_j}}
\tag{24}
$$

where μ_{A_i} is the membership function of A_i; and a_i, b_i and c_i are the parameters of the membership function.

The outputs of layer 2's nodes are the products of all incoming signals. In layer 3, the ratio of each output of layer 2 to the sum of all the outputs of layer 2 is calculated. The output data of layer 3 are called *normalised firing strengths*.

In layer 4, the output data are defined as:

$$O_{4i} = \bar{w}_i f_i \tag{25}$$

where $\bar{w}_i$ is the normalised firing strengths from layer 3 and f_i is the consequent parameter from the Tagaki-Sugeno system given in Equation (23).

The nodes in layer 5 calculate the sum of the incoming signals from layer 4. This layer also computes the overall output of the ANFIS algorithm.

The objective of gain scheduling is to determine the control gains K_x, K_i, K_p, K_{ff} and K_d as function of the altitude, airspeed and mass (three-dimensional interpolation). To simplify the learning process in the ANN, the ANFIS was only used for a three-dimensional interpolation (for airspeed and altitude). A linear interpolation was then used to estimate the control gains as function of mass.

Step 4: A performance analysis of the gain-scheduled controller is made. The local stability and robustness of the controller was investigated for unknown operating points and the nonlinear performance on the overall UAS-S45 model was tested as explained in the next Section 5.

5.0 Simulation results and discussion

In order to calculate the effectiveness of the proposed control schemes, several numerical simulations were performed for each flight condition. The random flight case considered in this section is defined by the airspeed $V = 39.76$m/s, altitude $= 6097$m and mass $= 53.11$kg. The values of the state, control and output matrices calculated for this flight case are given in Equations (1) and (2), as follows:

Longitudinal dynamics model matrices are:

$$\mathbf{A} = \begin{bmatrix} -0.0468 & 0.2359 & -1.8284 & -9.7513 \\ -0.3413 & -3.3721 & 41.1194 & -0.4463 \\ -0.1150 & -1.1861 & 0.3745 & -0.0213 \\ 0 & 0 & 1 & 0 \end{bmatrix}$$

$$\mathbf{B} = \begin{bmatrix} -0.0085 \\ 0.0424 \\ -0.1413 \\ 0 \end{bmatrix}, \mathbf{C} = \begin{bmatrix} 0 & 0 & 0 & 1 \end{bmatrix} \tag{26}$$

Lateral dynamics model matrices are:

$$\mathbf{A} = \begin{bmatrix} -0.2423 & 0.2954 & -50.3286 & 9.7613 \\ -0.0619 & -12.8788 & 0.8274 & 0 \\ 0.0870 & -0.2368 & -0.1602 & 0 \\ 0 & 1 & 0.0060 & 0 \end{bmatrix}$$

$$\mathbf{B} = \begin{bmatrix} 0 & 0.0386 \\ 0.6512 & 0.0074 \\ -0.0078 & -0.1628 \\ 0 & 0 \end{bmatrix}, \mathbf{C} = \begin{bmatrix} 0 & 0 & 0 & 1 \end{bmatrix} \tag{27}$$

Moreover, consider the next matrix for longitudinal GESO design,

$$\mathbf{b}_d = \begin{bmatrix} \mathbf{0}_{3\times1} \\ 1 \\ 0 \end{bmatrix}, i = 4, \ j = 1, \ m = 5 \text{ and } n = 1 \tag{28}$$
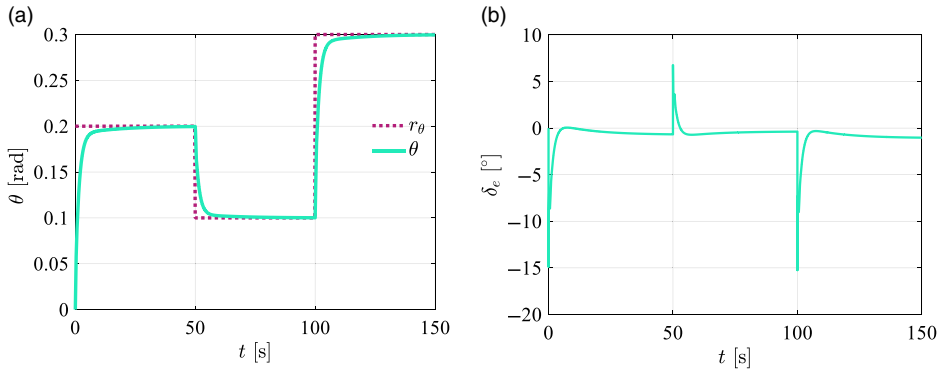
Figure 9. *Unperturbed pitch motion for the (a) trajectory tracking and (b) computed control input.*
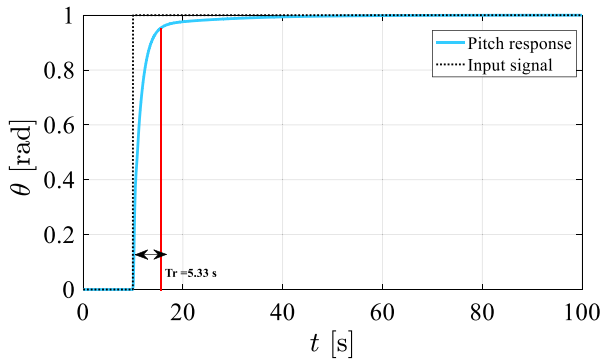

Figure 10. *Step response of the UAS-S45.*

and for lateral GESO design,

$$
\mathbf{b}_d = \begin{bmatrix} 0 \\ 1 \\ \mathbf{0}_{3 \times 1} \end{bmatrix}, \ i = 4, \ j = 2, \ m = 5 \text{ and } n = 2 \tag{29}
$$

The following reference profile was assigned to the longitudinal dynamics model:

$$
r_\theta(t) = \begin{cases} 0.2 \text{ rad}, & 0 \leq t \leq 50 \sec \\ 0.1 \text{ rad}, & 30 < t \leq 100 \sec \\ 0.3 \text{ rad}, & t > 150 \sec \end{cases} \tag{30}
$$

where step functions were established as references in order to assess the control scheme capabilities. Figures 9a and 9b show the trajectory tracking and the computed control inputs, respectively; a proper trajectory tracking was achieved under the action of the control input computed by the proposed control approach for an unperturbed motion. In addition to the accurate tracking, the criteria defined in Table 3 were also met. Figure 10 shows a step response of the UAS-S45. From this figure, the step response parameters are: (time response) $T_r = 5.33$s, (steady state error), $e_p = 10^{-3}$ and (overshoot), $D = 0$ which all satisfy the needed criteria.

The UAS was, thus, commanded to track the reference profile given in Equation (30) while it was subjected to the effects of disturbances. The disturbances affecting the pitch and roll motion are given by
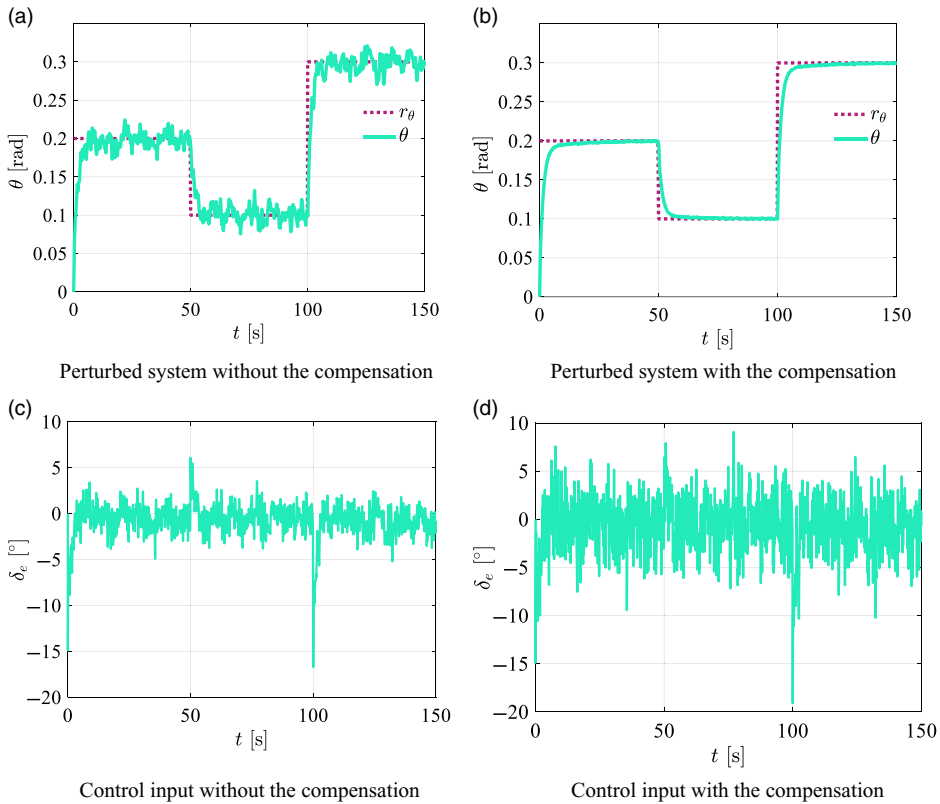
Figure 11. Pitch trajectory tracking.

d_q and d_r, respectively; which are assumed to be unknown but bounded parameters. The Dryden wind turbulence model was used to generate both disturbances. The MIL-F-8785C provides the model for the pitch disturbance as shown in the next equation:

$$d_q(\omega) = \frac{\left(\frac{\omega}{V}\right)^2}{1 + \left(\frac{4b\omega}{\pi V}\right)^2} \cdot \Phi_w(\omega) \tag{31}$$

$$\Phi_w(\omega) = \frac{\sigma_w^2 L_w}{\pi V} \cdot \frac{1 + 3\left(L_w \frac{\omega}{V}\right)^2}{\left[1 + \left(L_w \frac{\omega}{V}\right)^2\right]^2} \tag{32}$$

In Equations (31) and (32), σ_w is the turbulence intensity, L_w is the scale length, b is the span of the aircraft ω is the circular frequency and V is the airspeed.

The closed-loop dynamic responses for pitch motion are portrayed in Fig. 11. Overall, the results show that the control scheme offers a very good performance, but this scheme is not adequate when disturbances are included in the simulation without the GESO. On the other hand, when the GESO controller is used, an acceptable level of disturbance attenuation is achieved while reachable control inputs are computed. It must be noted that the control inputs effort does not saturate the actuators capabilities, since the maximum and minimum elevator deflections are $-40°$ and $40°$, respectively. The Dryden disturbance model used in this test was applied with a very high frequency to show the ability of the controller. It results in an increase of the actuator workload. The main goal of the test was to show the ability of the controller to cope the disturbances and that the actuator is not saturated.
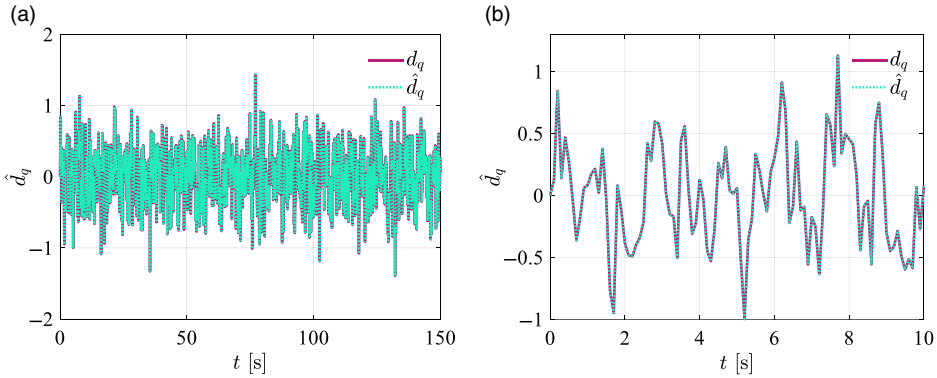
Figure 12. *Disturbances affecting the longitudinal motion, real (solid line) and GESO-estimated (dashed line). (a) disturbance over the simulation time, (b) zoom of the disturbance between 0 to 10s.*
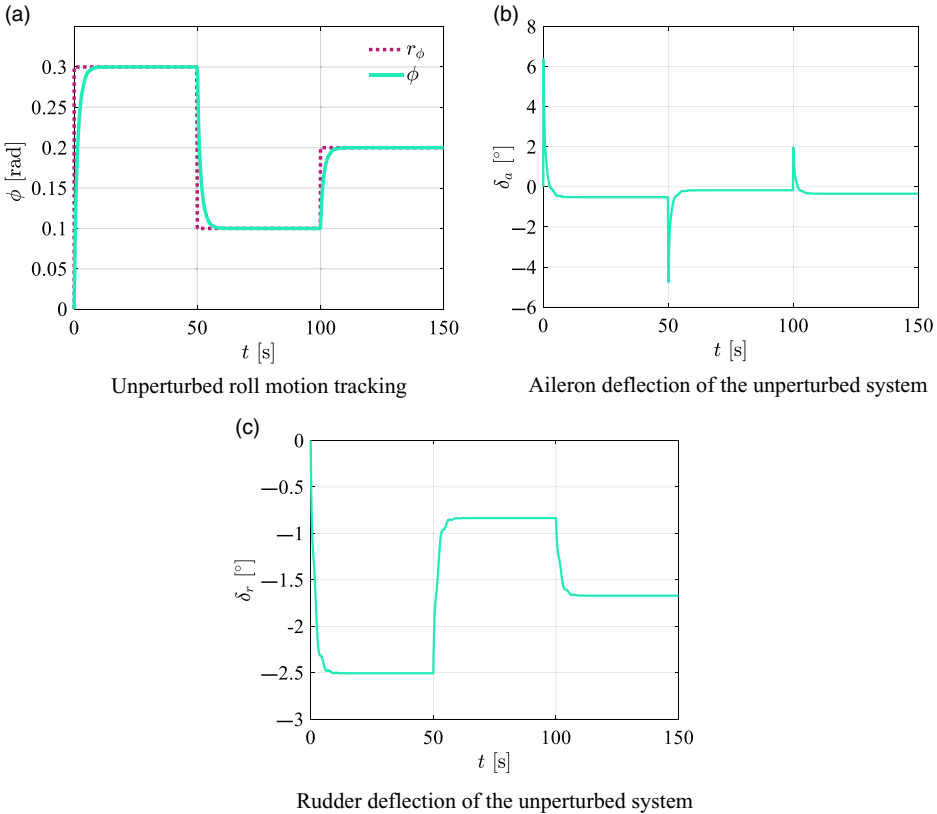

Unperturbed roll motion tracking

Aileron deflection of the unperturbed system

Rudder deflection of the unperturbed system

Figure 13. *Unperturbed roll motion.*

The real longitudinal disturbances and the disturbances estimated by the GESO are portrayed in Fig. 12 in solid and dashed lines, respectively. The ability of the estimated disturbance to track the real disturbance shows that the observer gain expressed in Equation (22) was selected properly.

Table 5. *Numbers and percentages of interpolation and validation data points*

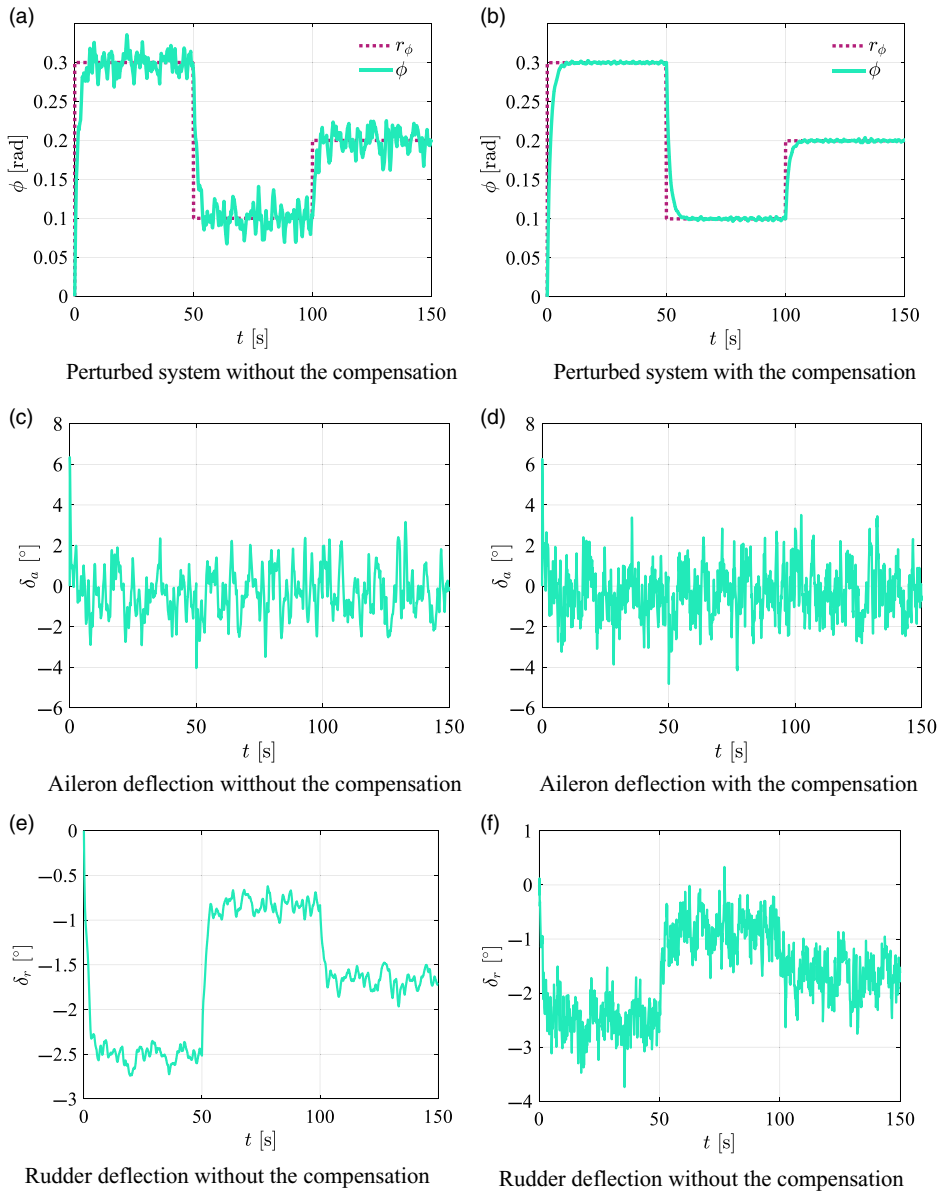|	
Number of interpolation data points	216
Number of validation data points	50
Success percentage (%) for longitudinal dynamics	84%
Success percentage (%) for lateral dynamics	92%

Figure 14. *Roll trajectory tracking.*

The proposed control scheme allows the system to deal with the trajectory tracking problem even in the presence of external disturbances, thanks to the action of the disturbance rejection mechanism provided by the GESO.
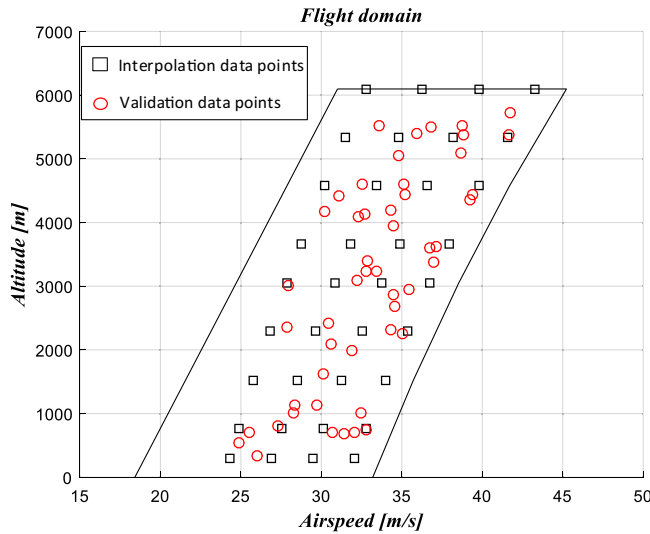
Figure 15. *Interpolation and validation data points.*

The control law for the lateral motion of the UAS-S45 was also defined. The scheme allows the aileron and rudder deflections to be used as control inputs for the roll motion (multiple inputs - single output). Two equivalent control laws, as the ones shown in Equation (3), are needed to deal with the trajectory tracking problem and disturbance rejection. The reference profile defined in Equation (33) is the 'planned reference' in which both the δ_a and δ_r control inputs are used to regulate the roll motion.

$$r_\phi(t) = \begin{cases} 0.2 \text{ rad}, & 0 \le t \le 50 \text{ sec} \\ 0.1 \text{ rad}, & 30 < t \le 100 \text{ sec} \\ 0.3 \text{ rad}, & t > 150 \text{ sec} \end{cases} \tag{33}$$

The tracking of the roll reference, in which a properly closed-loop system performance was achieved, is portrayed in Fig. 13. In the same way, the control inputs vary softly, which avoids actuator saturation. Nevertheless, disturbances were not included in this simulation.

For the longitudinal dynamics, the MIL-F-8785C specification of the Dryden wind turbulence model was used for the lateral disturbance modeling, as follows:

$$d_r = \frac{\left(\frac{\omega}{V}\right)^2}{1 + \left(\frac{3b\omega}{\pi V}\right)^2} \cdot \Phi_v(\omega) \tag{34}$$

$$\Phi_v(\omega) = \frac{\sigma_v^2 L_v}{\pi V} \cdot \frac{1 + 3\left(L_v \frac{\omega}{V}\right)^2}{\left[1 + \left(L_v \frac{\omega}{V}\right)^2\right]^2} \tag{35}$$

The system's dynamic response is shown in Fig. 14, where the uncompensated (Fig. 14a) and compensated (Fig. 14b) responses are portrayed. The system governed by the GESO approach guarantees a stable performance and attains a proper trajectory tracking.

Figure 14a, 14c and 14e shows respectively the perturbed system, the aileron control input and the rudder control input without compensation, and Fig. 14b, 14d and 14f shows respectively the perturbed system, the aileron control input and the rudder control input with compensation. The obtained roll angle still agrees with the desired angle even in the presence of disturbance. Despite an increase in the magnitude of the computed aileron and rudder control inputs, the actuators are not saturated (Fig. 14d
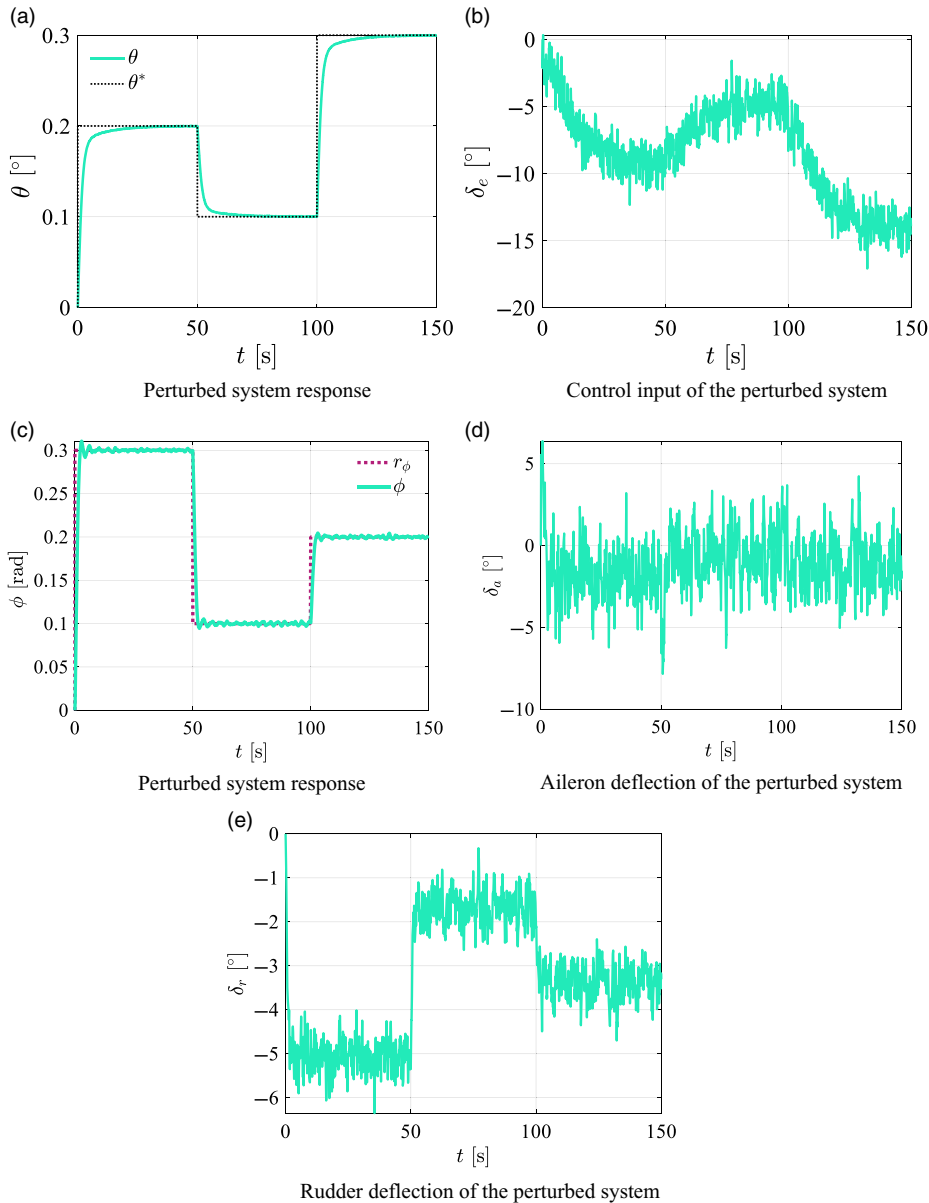
Figure 16. *Pitch and roll trajectories tracking using the nonlinear controller.*

and 14f). This fact means that the proposed robust control strategy is capable of performing the trajectory tracking task in the presence of significant external wind disturbances affecting the UAS-S45's motion.

To analyse the accuracy of the nonlinear controller, a cross validation was performed for the gain scheduling methodology. A set of 50 data points, selected randomly, was used for this validation as illustrated in Fig. 15. The interpolation data points shown in Fig. 15 represent the data used to train the ANFIS gain-scheduling model. For each validation point (which is a flight condition), the linearised model was obtained, and the controller gains were estimated using the ANFIS model. The data points were considered successful if the controlled system verified all flight qualities requirements described in Section 3.1. Table 5 shows the number and percentages of validated data points for the longitudinal and

lateral dynamics models. The results indicate high success rates of 84% for the longitudinal dynamics, and 92% for the lateral dynamics models.

Figures 16a and 16b show the pitch trajectory tracking and the control input for a successful validation point. The disturbances calculated in Equation (31) and in Equation (32) were injected in the longitudinal dynamic model to evaluate its disturbance rejection capability. The results show that the tracking capability as well as the robustness of the nonlinear controller are still highly efficient. Figure 16b shows that the control input can reject the sinusoidal disturbance while remaining inside the range of the elevator deflection $[-40°, 40°]$.

Figure 16c and 16d show the roll trajectory tracking and the control input for a successful validation point. The disturbance described in Equation (34) and in Equation (35) was injected in the system to evaluate its robustness. The results also show a very good tracking performance with an efficient disturbance rejection.

Conclusion

A design methodology to obtain a low-order robust controller was described in this paper. The poor robustness of the optimal controller, the high order of the robust controller, and the lack of data of the neural network controller were the main challenges which needed to be solved in this work. The methodology was developed in three steps. The first step concerned the design of a Linear Quadratic Regulator (LQR) that used a selection technique for the weight matrices. In the second step, a Proportional-Integral with reference Feed-Forward (PI-FF) was added to the controller, in order to provide very good tracking capability, and slow dynamics variations robustness. In the third step, a Generalised Extended State Observer (GESO) was designed for both disturbances gain calculation and estimation. The obtained linear controller was thus extended to obtain a nonlinear controller using a Gain Scheduling based on the ANFIS method. Several numerical simulations were performed to highlight the feasibility and efficiency of the proposed methodology. The results obtained showed a very good tracking and stability performance even under disturbances. The nonlinear controller also showed efficient results, but there is a need to increase the number of interpolation points close to the boundary of the flight envelope in order to improve the results. The obtained results, thus, proved that the proposed methodology is very good for the design of a UAS-S45 flight controller.

References

[1] Eren, U., Prach, A., Koçer, B.B., Raković, S.V., Kayacan, E. and Açıkmeşe, B. Model predictive control in aerospace systems: Current state and opportunities, *J. Guid. Control Dyn.*, 2017, **40**, pp 1541–1566. https://doi.org/10.2514/1.G002507

[2] Valyou, D., Ceruti, A., Miller, J., Pawlowski, B., Marzocca, P. and Tranchitella, M. Design, Optimisation, Performances and Flight Operation of an All Composite Unmanned Aerial Vehicle. SAE International, 2013.

[3] Aubeelack, H. and Botez, R.M. Simulation study of the aerodynamic force distributions on the UAS-S45 Baalam wing with an upswept blended winglet, *INCAS Bull.*, 2019, **11**, pp 21–38.

[4] Sugar Gabor, O., Koreanschi, A. and Botez, R.M. Numerical study of UAS-S4 Éhecatl aerodynamic performance improvement obtained with the use of a morphing wing approach, 33rd AIAA Applied Aerodynamics Conference, p 2259, American Institute of Aeronautics and Astronautics, 2015.

[5] Segui, M., Kuitche, M. and Botez, R.M. Longitudinal aerodynamic coefficients of hydra technologies UAS-S4 from geometrical data, AIAA Modeling and Simulation Technologies Conference, p 0579, American Institute of Aeronautics and Astronautics, 2017.

[6] Kammegne, M.J.T., Grigorie, L.T., Botez, R.M. and Koreanschi, A. Design and wind tunnel experimental validation of a controlled new rotary actuation system for a morphing wing application, Proc. Inst. Mech. Eng. G J. Aerosp. Eng., 2016, **230**, pp 132–145. https://doi.org/10.1177/0954410015588573

[7] Botez, R.M., Kammegne, M.J.T. and Grigorie, L.T. Design, numerical simulation and experimental testing of a controlled electrical actuation system in a real aircraft morphing wing model, *Aeronaut. J.*, 2015, **119**, pp 1047–1072. https://doi.org/10.1017/S0001924000011131

[8] Li, B., Zhang, Y., Ge, Y., Shao, Z. and Li, P. Optimal control-based online motion planning for cooperative lane changes of connected and automated vehicles, Presented at the 2017 IEEE/RSJ International Conference on Intelligent Robots and Systems (IROS), Vancouver, BC September, 2017.

[9] Frost, S., Taylor, B. and Bodson, M. Investigation of optimal control allocation for gust load alleviation in flight control, Presented at the AIAA Atmospheric Flight Mechanics Conference, Minneapolis, Minnesota, 2012.

[10] Zhen, Z., Jiang, J., Wang, X. and Gao, C. Information fusion based optimal control for large civil aircraft system, *ISA Trans.*, 2015, **55**, pp 81–91. https://doi.org/10.1016/j.isatra.2014.09.017

[11] Vinodh Kumar, E., Raaja, G.S. and Jerome, J. Adaptive PSO for optimal LQR tracking control of 2 DoF laboratory helicopter, *Appl. Soft Comput.*, 2016, **41**, pp 77–90. https://doi.org/10.1016/j.asoc.2015.12.023

[12] Kálmán, R.E. Contributions to the theory of optimal control, Presented at the Bol. Soc. Mat. Mexicana, 1960.

[13] Doyle, J.C. Guaranteed margins for LQG regulators, *IEEE Trans. Automat. Control*, 1978, **23**, pp 756–757.

[14] Starr, A.W. and Ho, Y.C. Nonzero-sum differential games, *J. Optim. Theory Appl.*, 1969, **3**, pp 184–206. https://doi.org/10.1007/BF00929443

[15] Rosenbrock, H. and McMorran, P. Good, bad, or optimal? *IEEE Trans. Automat. Control*, 1971, **16**, pp 552–554. https://doi.org/10.1109/TAC.1971.1099822

[16] Sadeghzadeh, I., Chamseddine, A., Theilliol, D. and Zhang, Y. Linear parameter varying control synthesis : State feedback versus H∞ technique with application to quadrotor UAV, Presented at the 2014 International Conference on Unmanned Aircraft Systems (ICUAS), Orlando, FL May, 2014.

[17] Balas, M. and Frost, S. Robust adaptative control with disturbance rejection for linear infinite dimensional systems, AIAA Guidance, Navigation, and Control Conference 2012, 2012.

[18] Boughari, Y., Botez, R.M., Ghazi, G. and Theel, F. Flight control clearance of the Cessna Citation X using evolutionary algorithms, *Proc. Inst. Mech. Eng. G J. Aerosp. Eng.*, 2017, **231**, pp 510–532. https://doi.org/10.1177/0954410016640821

[19] Liu, X., Sun, Q. and Cooper, J.E. LQG based model predictive control for gust load alleviation, *Aerosp. Sci. Technol.*, 2017, **71**, pp 499–509. https://doi.org/10.1016/j.ast.2017.10.006

[20] Pavel, M., Shanthakumaran, P., Stroosma, O., Chu, Q., Wolfe, M. and Cazemier, H. Development of advanced flight control laws for the AH-64 Apache helicopter: Sketches from the work of TU Delft-Boeing project in SIMONA simulator, 72nd Annual Forum of the American Helicopter Society: West Palm Beach, USA, 2016.

[21] Pavel, M., Shanthakumaran, P., Chu, Q., Stroosma, O., Wolfe, M. and Cazemier, H. Incremental nonlinear dynamic inversion for the Apache AH-64 helicopter control. *J. Am. Helicopter Soc.*, 2020, **65**. https://doi.org/10.4050/JAHS.65.022006

[22] Simplicio, P., Pavel, M., Van Kampen, E.-J. and Chu, Q. An acceleration measurements-based approach for helicopter nonlinear flight control using incremental nonlinear dynamic inversion, *Control Eng. Pract.*, 2013, **21**, pp 1065–1077. https://doi.org/10.1016/j.conengprac.2013.03.009

[23] Obinata, G. and Anderson, B.D.O. Methods for Model Reduction. In: *Model Reduction for Control System Design. Communications and Control Engineering.* pp. 1–59. Springer, London, 2012. https://doi.org/10.1007/978-1-4471-0283-0_1

[24] Liu, Z.X., Yuan, C., Zhang, Y. and Luo, J. A learning-based fuzzy LQR control scheme for height control of an unmammed quadrotor helicopter, Presented at the 2014 International Conference on Unmanned Aircraft Systems (ICUAS), Orlando, FL May, 2014.

[25] Magar, K.T., Balas, M., Frost, S. and Li, N. Adaptive state feedback: Theory and application for wind turbine control, *Energies*, 2017, **10**, p 2145. https://doi.org/10.3390/en10122145

[26] Ceruti, A., Rossi, V. and Saggiani, G.M. A fuzzy logic autopilot development for a light twin engine aircraft in the approach flight condition, Presented at the ICAS 2002 Congress, 2002.

[27] Hušek, P. and Narenathreyas, K. Aircraft longitudinal motion control based on Takagi–Sugeno fuzzy model, *Appl. Soft Comput.*, 2016, **49**, pp 269–278. https://doi.org/10.1016/j.asoc.2016.07.038

[28] Duong, M.Q., Grimaccia, F., Leva, S., Mussetta, M. and Ogliari, E. Pitch angle control using hybrid controller for all operating regions of SCIG wind turbine system, *Renew. Energy,* 2014, **70**, pp 197–203. https://doi.org/10.1016/j.renene.2014.03.072

[29] Duong, M.Q., Grimaccia, F., Leva, S., Mussetta, M. and Le, K.H. Improving transient stability in a grid-connected squirrel-cage induction generator wind turbine system using a fuzzy logic controller, *Energies*, 2015, **8**, pp 6328–6349. https://doi.org/10.3390/en8076328

[30] Grimaccia, F., Mussetta, M. and Zich, R. Neuro-fuzzy predictive model for PV energy production based on weather forecast, 2011 IEEE International Conference on Fuzzy Systems (FUZZ-IEEE 2011), pp 2454–2457, 2011.

[31] Wu, D., Chen, M. and Gong, H. Adaptive neural flight control for an aircraft with time-varying distributed delays, *Neurocomputing,* 2018, **307**, pp 130–145. https://doi.org/10.1016/j.neucom.2018.04.038

[32] Fareh, R., Al-Shabi, M., Bettayeb, M. and Ghommam, J. Robust active disturbance rejection control for flexible link manipulator, *Robotica*, 2020, **38**, pp 118–135.

[33] Han, J. From PID to active disturbance rejection control, *IEEE Trans. Ind. Electron.*, 2009, **56**, pp 900–906.

[34] Li, S., Yang, J., Chen, W.-H. and Chen, X. Generalized extended state observer based control for systems with mismatched uncertainties, *IEEE Trans. Ind. Electron.*, 2011, **59**, pp 4792–4802.

[35] Fethalla, N., Saad, M., Michalska, H. and Ghommam, J. Robust observer-based dynamic sliding mode controller for a quadrotor UAV, *IEEE Access*, 2018, **6**, pp 45846–45859.

[36] Ghommam, J., Mnif, F. and Derbel, N. Global stabilisation and tracking control of underactuated surface vessels, *IET Control Theory Appl.*, 2010, **4**, pp 71–88.

[37] Shi, D., Wu, Z. and Chou, W. Generalized extended state observer based high precision attitude control of quadrotor vehicles subject to wind disturbance, *IEEE Access*, 2018, **6**, pp 32349–32359.

[38] Pawar, S.N., Chile, R.H. and Patre, B.M. Design of generalized extended state observer based control for nonlinear systems with matched and mismatched uncertainties, 2017 Indian Control Conference (ICC), pp 65–71, IEEE, 2017.

[39] Leggett, D. and Cord, T. Flying qualities demonstration maneuvers, Biennial Flight Test Conference, p 2113, 1994.

[40] Klyde, D.H., Schulze, C.P., Miller, J.P., Manriquez, J.A., Kotikalpudi, A., Mitchell, D.G., Seiler, P.J., Regan, C., Taylor, B. and Olson, C. Defining Handling Qualities of Unmanned Aerial Systems: Phase II Final Report. National Aeronautics and Space Administration, Hampton, Virginia, 2020.

[41] Li, T., Zhang, S., Yang, H., Zhang, Y. and Zhang, L. Robust missile longitudinal autopilot design based on equivalent-input-disturbance and generalized extended state observer approach, *Proc. Inst. Mech. Eng. G J. Aerosp. Eng.*, 2015, **229**, pp 1025–1042.

[42] Kang, H.-S., Kim, Y.-T., Hyun, C.-H. and Park, M. Generalized extended state observer approach to robust tracking control for wheeled mobile robot with skidding and slipping, *Int. J. Adv. Robot. Syst.*, 2013, **10**, p 155.

[43] Das, S. and Talole, S.E. GESO based robust output tracking controller for marine vessels, *Ocean Eng.*, 2016, **121**, pp 156–165.

[44] Zhou, Y., Huang, Z., Peng, J., Li, H. and Liao, H. A generalized extended state observer for supercapacitor state of charge estimation under disturbances, 2017 American Control Conference (ACC), pp 4029–4034, IEEE, 2017.

[45] Villaseñor, C., Gallegos, A.A., Gomez-Avila, J., López-González, G., Rios, J.D. and Arana-Daniel, N. Environment classification for unmanned aerial vehicle using convolutional neural networks, *Appl. Sci.*, 2020, **10**, p 4991. https://doi.org/10.3390/app10144991

[46] Kuitche, M.A.J. and Botez, R.M. Modeling novel methodologies for unmanned aerial systems: Applications to the UAS-S4 Ehecatl and the UAS-S45 Bálaam, *Chinese J. Aeronaut.*, 2019, **32**, pp 58–77. https://doi.org/10.1016/j.cja.2018.10.012

[47] Anton, N., Botez, R.M. and Popescu, D. Stability derivatives for a delta-wing X-31 aircraft validated using wind tunnel test data, *Proc. Inst. Mech. Eng. G J. Aerosp. Eng.*, 2011, **225**, 403–416. https://doi.org/10.1243/09544100JAERO799

[48] Popescu, D. Nouvelle Implémentation de la Procédure DATCOM pour le Calcul des Coefficients Aérodynamiques et des Dérivées de Stabilité dans le Domaine Subsonique de Vol, http://espace.etsmtl.ca/74/, 2009.

[49] Anton, N., Botez, R. and Popescu, D. New methodologies for aircraft stability derivatives determination from its geometrical data, AIAA Atmospheric Flight Mechanics Conference, p 6046, American Institute of Aeronautics and Astronautics, Chicago, Illinois, 2009.

[50] Mitchell, D.G., Hoh, R.H., Aponso, B.L. and Klyde, D.H. Proposed Incorporation of Mission-Oriented Flying Qualities into MIL-STD-1797A. Systems Technology Inc Hawthorne CA, 1994.

[51] US Military: MIL-F-8785C, Military Specification: Flying Qualities Of Piloted Airplanes, 1980.

[52] Cook, M.V. Chapter 5 - The Solution of the Equations of Motion. In: *Flight Dynamics Principles* (Third Edition). pp. 109–145. Butterworth-Heinemann, Oxford, 2013. https://doi.org/10.1016/B978-0-08-098242-7.00005-5

[53] Stevens, B.L. and Lewis, F.L. *Aircraft Control and Simulation*, John Wiley & Sons, 2003, Hoboken, N.J.

[54] Phillips, W.F. *Mechanics of Flight*, John Wiley & Sons, Inc, 2009, New Jersey.

[55] Choi, J.W. and Seo, Y.B. LQR design with eigenstructure assignment capability [and application to aircraft flight control, *IEEE Trans. Aerosp. Electron. Syst.*, 1999, **35**, pp 700–708. https://doi.org/10.1109/7.766949

[56] Vepa, R. *Flight Dynamics, Simulation, and Control : For Rigid and Flexible Aircraft*, CRC Press, 2014, Boca Raton.

[57] Ashraf, A., Mei, W., Gaoyuan, L., Anjum, Z. and Kamal, M.M. Design linear feedback and LQR controller for lateral flight dynamics of F-16 aircraft, 2018 International Conference on Control, Automation and Information Sciences (ICCAIS), pp 367–371, 2018.

[58] Reznik, L., Ghanayem, O. and Bourmistrov, A. PID plus fuzzy controller structures as a design base for industrial applications, *Eng. Appl. Artif. Intell.*, 2000, **13**, pp 419–430. https://doi.org/10.1016/S0952-1976(00)00013-0

[59] Saussié, D., Saydy, L. and Akhrif, O. Longitudinal flight control design with handling quality requirements, *Aeronaut. J.*, 2006, **110**, pp 627–637. https://doi.org/10.1017/S0001924000001494

[60] Li, S., Yang, J., Chen, W. and Chen, X. Generalized extended state observer based control for systems with mismatched uncertainties, *IEEE Trans. Ind. Electron.*, 2012, **59**, pp 4792–4802. https://doi.org/10.1109/TIE.2011.2182011

[61] Rugh, W.J. and Shamma, J.S. Research on gain scheduling, *Automatica*, 2000, **36**, pp 1401–1425. https://doi.org/10.1016/S0005-1098(00)00058-3

[62] Jang, J.-S.R. ANFIS: Adaptive-network-based fuzzy inference system, *IEEE Trans. Syst. Man. Cybern.*, 1993, **23**, pp 665–685. https://doi.org/10.1109/21.256541

[63] Grigorie, T.L., Botez, R.M., Popov, A.V., Mamou, M. and Mébarki, Y. A hybrid fuzzy logic proportional-integral-derivative and conventional on-off controller for morphing wing actuation using shape memory alloy part 1: Morphing system mechanisms and controller architecture design, *Aeronaut. J.*, 2012, **116**, pp 433–449. https://doi.org/10.1017/S0001924000006977

[64] Grigorie, T.L. and Botez, R.M. Adaptive neuro-fuzzy inference system-based controllers for smart material actuator modelling, *Proc. Inst. Mech. Eng. G J. Aerosp. Eng.*, 2009, **223**, pp 655–668. https://doi.org/10.1243/09544100JAERO522

[65] Grigorie, T.L. and Botez, R.M. Positioning monitoring improvement in a horizontal plane INS by using fuzzy logic data fusion for denoising of inertial sensors in redundant clusters, *Int. J. Fuzzy Syst. Adv. Appl.*, 2015, **2**, pp 33–40.

[66] Suparta, W. and Alhasa, K.M. Adaptive Neuro-Fuzzy Interference System. In: *Modeling of Tropospheric Delays Using ANFIS*, pp. 5–18. Springer International Publishing, 2016, Cham.